Study on Enlarging the Searching Scope of Staring Area and Tracking Imaging of Dynamic Targets by Optical Satellites

Li Jiang and Xiubin Yang

***Abstract*—Conventional optical satellite imaging, such as push-broom imaging, obtained static image and was unable to get the characteristic of dynamic target. Staring imaging can obtain dynamic image. However, the coverage of the image, limited by the field of view (FOV) of the payload, is within only a dozen square kilometers. In this paper, a regional searching model and a tracking algorithm are proposed to enlarge the searching scope of staring area and to instruct tracking imaging of dynamic targets with a small FOV. In order to enlarge the searching area, a mathematical model is designed by setting a virtual target position under the original target position. Considering the center of dynamic target as the target-missing quantity, the tracking algorithm is established to control the satellite attitude so as to ensure that the optical axis points to the target-missing quantity. Finally, the algorithm is verified through ground experiments and the conclusion is demonstrated through on-orbit experiments with the first video satellite of Jilin province(JL-1). Compared with conventional staring imaging, the range of searching imaging can be expanded by 8 times. When the attitude angle and angular velocity of the satellite are better than 0.05° and 0.08°/s, respectively, the tracking accuracy of the target center can be shorter than one pixel, and the image will be distinctly visible.**

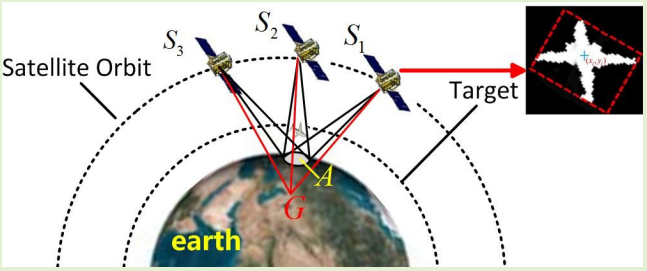

***Index Terms*— Dynamic targets, extended searching, tracking, imaging area, optical satellite.**

I. Introduction

With the rapid development of global commercial aerospace technology, new dynamic imaging modes are becoming the direction of space remote sensing for military and civilian applications. In recent years, it has happened several natural disasters and emergencies within hundreds of kilometers in china, such as the loss of Malaysia Airlines, Wen Chuan earthquake and other real-time events. These accidents have been still in the process of dynamic change for a period of time after the occurrence, so it is necessary to perceive the "uncertainty" of regional dynamic changes. For example, in the earthquake zone, traffic dynamic status should be quickly detected to guide the route of rescue vehicles; the verticality of high objects can be measured from different perspectives to analyze the safety factor [1]–[4].

So far, in order to obtain images from areas of hundreds of kilometers, the push-broom imaging mode is usually adopted by satellites along the tracking [5], [6], which has outstanding advantages such as high accuracy, good controllability, and strong anti-interference ability. However, the disadvantage of this imaging mode is that the satellite can only acquire a static image of the dynamic target during the imaging process, and cannot track and predict dynamic characteristics. For acquiring dynamic image, the attitude of the optical satellite is maneuvered to point to the target with fixed longitude and latitude, and then the method of multi-frame photography is used to observe the continuous change of the dynamic target from different perspectives. On the other hand, the staring imaging always focuses on one point and the FOV is limited within ten kilometers, which likes "looking at the earth in a straw". It is impossible to get the characteristics or rapid change of dynamic target within hundred kilometers [7]–[9].

Now, varieties of imaging methods are designed for dynamic awareness. Aimed at the image of Quick bird, Masahiro

Manuscript received September 10, 2020; revised October 9, 2020; accepted October 10, 2020. Date of publication October 16, 2020; date of current version January 15, 2021. This work was supported in part by the National Natural Science Foundation of China (NSFC) under Grant 61705222 and Grant 62005275 and in part by the Major Projects of the Ministry of Science and Technology under Grant 2016YFB0501202. The associate editor coordinating the review of this article and approving it for publication was Dr. Ioannis Raptis. *(Corresponding authors: Li Jiang; Xiubin Yang.)*

Li Jiang is with the Physics Department, Changchun University of Science and Technology, Changchun 130022, China (e-mail: jiangli@cust.edu.cn).

Xiubin Yang is with the Space New Technique Department, Changchun Institute of Optics, Fine Mechanics and Physics, Chinese Academy of Sciences, Changchun 130033, China (e-mail: yangxiubin@ciomp.ac.cn).

Digital Object Identifier 10.1109/JSEN.2020.3031626

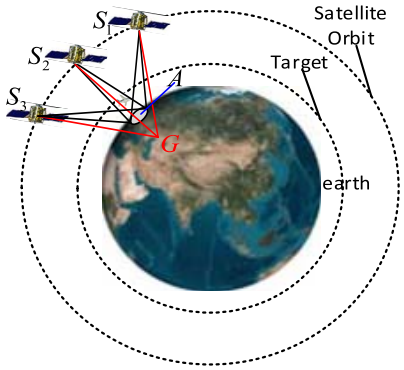

Fig. 1. Regional enlarging search imaging model of the dynamic target.

Etaya *et al.* calculated the velocity of the dynamic target by using the time threshold of multi-spectral sensor and the distance between the target and the shadow during the imaging, but the errors of this method are very large because the time threshold is short and the distance is close [10]. Wang Yamin *et al.* expanded the satellite coverage along the orbit by dividing the imaging strip area, and built the overlap rate of the frames and adjusting satellite attitude. Although this method improved the area of observation in large coverage, it strictly depended on the ground task planning and cannot track dynamic target in real time[11].

Based on these previous works, a virtual target position is set under the original target position in this paper. The precise attitude equations are established and the tracking parameters based on the target-missing quantity are analyzed to achieve distinct imaging. This technology can be used to find and track dynamic targets in large areas.

II. The Regional Search Imaging Model

In order to solve the problem of limited coverage area caused by narrow FOV of the satellite, a large regional search imaging model is designed. In this mode, a virtual point G that exists a certain distance under the surface A is set, and the satellite(S) can stare at the target point G from different perspectives (S_1, S_2, S_3) by adjusting its attitude, as shown in Fig. 1. In this way, the scope of staring is enlarged from a small original coverage to an arc surface, which greatly increases the search imaging range in a narrow FOV.

A. Calculation of Enlarging Coverage L and Overlap Rate η

In order to change the imaging range from the original coverage a to the enlarged coverage L, the target point G is virtually set as shown in Fig. 2. The longitude and latitude of the point G which projects on the surface is consistent with the original target point A. The distance from G to A is h, the orbit height of the satellite is H, the imaging range of the camera is $a \times a = S$, and the radius of the earth is R. The relationship between the enlarging coverage L and the distance h is detailed shown in Fig. 3. When the satellite pitch angle from the point G is θ, the angle γ and the coverage L are calculated according to the sine theorem of the triangle as follows:

$$\phi = 180 - \arcsin\left(\frac{(R+H)\times\sin\theta}{(R-h)}\right) \tag{1}$$

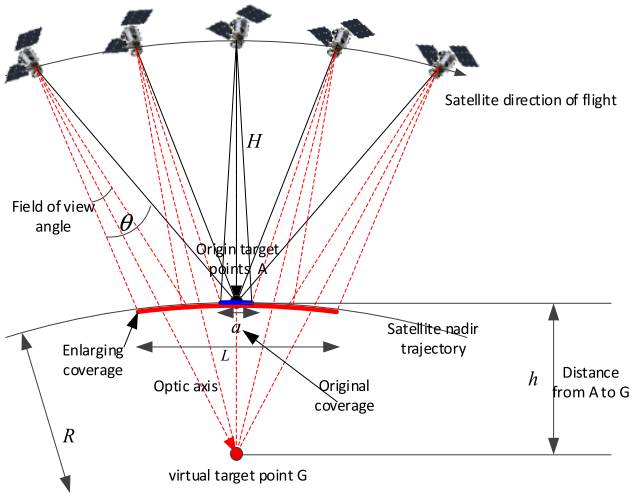

Fig. 2. Schematic diagram for expanded search and tracking imaging mode.

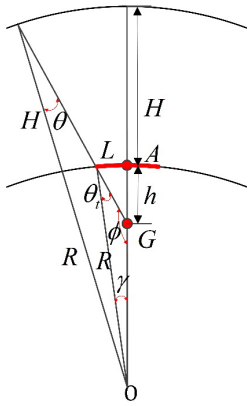

Fig. 3. The relationship between the enlarging coverage L and the distance h.

$$\theta_t = \arcsin\left(\frac{(R-h)\times\sin\phi}{R}\right) \tag{2}$$

$$\gamma = 180 - \phi - \theta_t \tag{3}$$

$$f(\theta) = 2R\gamma \tag{4}$$

The extended coverage can dramatically improve the visible range and reduce the overlap rate of two continuous frames. In order to optimize the balance between frame overlap rate η and the enlarging coverage L, the inter-frame overlap rate η is selected not less than 90%. When the angular velocity of the satellite is ω, the pitch angle of the satellite is $\pm\theta_0^\circ$, the frame frequency of the imaging is N and the inter-frame time is $t = 1/N$. The overlap of frames is shown in Fig. 4. The function of the frame overlap rate can be expressed as follows:

$$\eta = 1 - \frac{f(\theta_0) - f(\theta_0 + \omega t)}{a} \tag{5}$$

B. Satellite Pointing Attitude Analysis

The satellite should accurately point to the virtual target G during the process of staring imaging. Therefore, it is

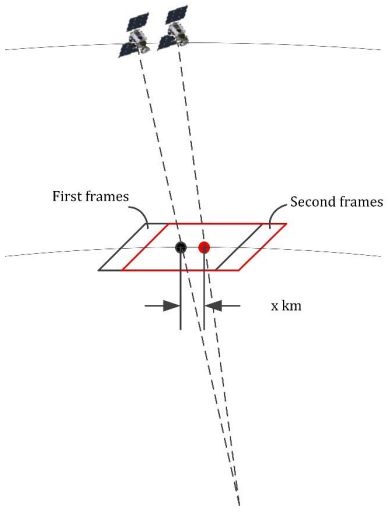

Fig. 4. Schematic diagram of the overlap between two continuous frames.

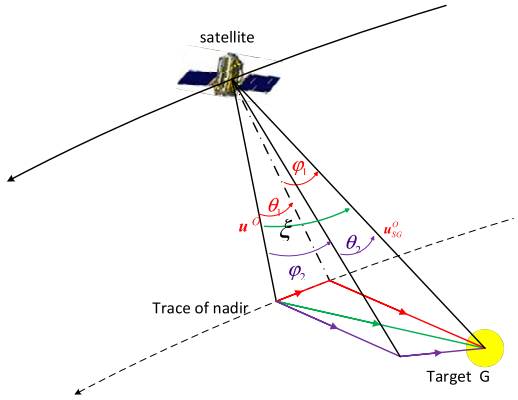

Fig. 5. Maneuver path selection of satellite attitude.

necessary to precisely establish the pointing model between the optical axis of the camera and the virtual target G, so as to ensure that the optical axis vector $\mathbf{u}^o$ always coincides with the observation vector $\mathbf{u}_{SG}^o$, and then make sure the angular path of satellite maneuver is the shortest [12]–[14], as shown in Fig. 5.

There are countless maneuvering paths to reach the desired attitude from the three-axis stability for the satellite which precisely points to the virtual target G [15], [16]. The shortest maneuvering path is selected according to the definition of the quaternion. The expected quaternion $\mathbf{Q}_c$ of the satellite's body coordinate system relative to the orbital coordinate system can be expressed as follows[17]:

$$\mathbf{Q}_c = \left[\cos\frac{\xi}{2} \quad \mathbf{e}\sin\frac{\xi}{2}\right]^{\mathrm{G}} = [\,q_{c0} \quad q_{c1} \quad q_{c2} \quad q_{c3}\,]^G \tag{6}$$

where ξ denotes the angle between the observation vector $\mathbf{u}_{SG}^o$ and the optical axis $\mathbf{u}^o$, and $\mathbf{e}$ is perpendicular to the vectors $\mathbf{u}_{SG}^o$ and $\mathbf{u}^o$:

$$\xi = \arccos\frac{\mathbf{u}^O \cdot \mathbf{u}_{SG}^O}{|\mathbf{u}^O| \cdot |\mathbf{u}_{SG}^O|} \tag{7}$$

$$\mathbf{e} = \frac{\mathbf{u}^O \times \mathbf{u}_{SG}^O}{|\mathbf{u}^O \times \mathbf{u}_{SG}^O|} \tag{8}$$

First, the optical axis vector $\mathbf{u}^o$ is calculated based on the satellite position vector, and then the unit vector $\mathbf{u}_{SG}^o$ of the observation vector in the orbital coordinates can be expressed as follows:

$$\mathbf{u}_{SG}^O = \frac{\mathbf{r}_{SG}^O}{|\mathbf{r}_{SG}^O|} \tag{9}$$

$$\mathbf{r}_{SG}^O = \mathbf{A}_I^o\left(\mathbf{r}_G^I - \mathbf{r}_S^I\right) \tag{10}$$

where $\mathbf{A}_I^o$ is the coordinate transformation matrix from the earth inertial coordinate system to the orbital coordinate system, $\mathbf{r}_S^I$ denotes the position vector of the satellite in the earth inertial coordinate system, and $\mathbf{r}_G^I$ represents the position vector of the target in the earth inertial coordinate system. The observation target is represented by the longitude α and latitude β on the earth surface. The target point G can be expressed in the earth inertial coordinate system I which is given by:

$$\mathbf{r}_G^I = \begin{bmatrix} x_G^I \\ y_G^I \\ z_G^I \end{bmatrix} = |\mathbf{r}_G| \cdot \begin{bmatrix} \cos\beta\cos\alpha \\ \cos\beta\sin\alpha \\ \sin\beta \end{bmatrix} \tag{11}$$

With $\alpha = \lambda + G_0 + \omega(t - t_0)$. Here, λ denotes the geographic latitude, G_0 represents the Greenwich star time angle, ω is the earth rotation velocity, and $|\mathbf{r}_G|$ is the length of the vector $\mathbf{r}_G$ from the target G to the center of earth O. And $a_e = 6378.137$ km (Earth's long half-axis), $b_e = 6356.7523$ km. (Earth's short half-axis). The radius of the earth's center is determined only by the latitude of the earth's center and can be written as

$$\begin{aligned} |\mathbf{r}_G| &= \sqrt{\frac{a_e^2 \cdot b_e^2 \cdot (1 + \tan^2\beta)}{b_e^2 + a_e^2 \cdot \tan^2\beta}} \\ &= \frac{a_e \cdot b_e}{\sqrt{a_e^2 \cdot \sin^2\beta + b_e^2 \cdot \cos^2\beta}} \end{aligned} \tag{12}$$

$\mathbf{Q}_c$ is the expected quaternion which satellite maneuvers to target G. The maneuvering Euler axis is perpendicular to the observation vector $\mathbf{u}_{SG}^o$ and the optical axis vector $\mathbf{u}^o$. There are no angular velocity components between $\mathbf{u}^o$ and $\mathbf{u}_{SG}^o$, so the maneuvering path of satellite is the shortest angular distance. When satellite rotates in a 3-1-2 order, the expected yaw angle, pitch angle and roll angle of the satellite which in body coordinate system relative to orbital coordinate system are obtained. The corresponding formulas are shown as follows:

$$\begin{cases} \psi = arctan\left[-\dfrac{2(q_1q_2 + q_3q_4)}{-q_1^2 + q_2^2 - q_3^2 + q_4^2}\right] \\ \varphi = arcsin\left[2\left(q_2q_3 - q_1q_4\right)\right] \\ \theta = arctan\left[-\dfrac{2\left(q_1q_3 + q_2q_4\right)}{-q_1^2 - q_2^2 + q_3^2 + q_4^2}\right] \end{cases} \tag{13}$$

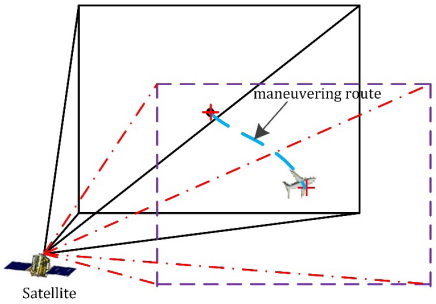

Fig. 6. Target-missing quantity extracted and attitude tracking guided.

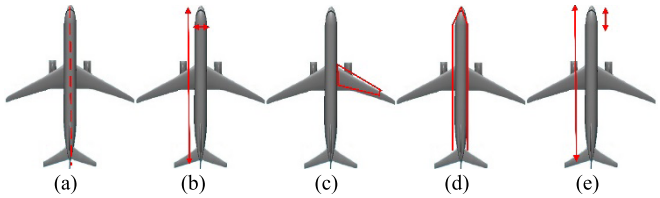

Fig. 7. Aerodynamic configuration characteristics of aircraft. (a) Symmetrical characteristic; (b) ratio of aspect; (c) ratio of wing trapezoid; (d) ratio of body shape; (e) ratio of leading-edge.

III. Attitude Tracking Guided by Target-Missing Quantity

Owing to the complex characteristics of dynamic targets, real-time tracking is a very high challenge. In order to facilitate on-orbit application, the simple and reliable conventional methods is proposed. Target-missing quantity is extracted to provide guidance data for satellite tracking control, as shown in Fig. 6.

A. Moving Target Acquisition by Improved SIFT Method

In order to quickly acquire moving targets from regional images, an improved Scale-invariant feature transform (SIFT) algorithm is adopted in this paper. This algorithm is based on aerodynamic configuration characteristics of aircraft [18], [19]. According to the characteristics of aircraft, such as symmetry, ratio of aspect, ratio of wing trapezoid, ratio of body shape and ratio of leading-edge, which can constrain different types of aircraft, as shown in Fig. 7(a) ∼ (e), the SIFT algorithm is utilized to distinguish aircrafts with certain number of samples.

B. Image Binarization Processing

In order to quickly distinguish the shape of target, the OTSU method, which is proposed by Nobuyki Otsu for binary segmentation threshold, is used to determine the optimal threshold of aircraft. The pixel values are 255 and 0, respectively, between the target objects and the background image. And then the opening operation (a kind of morphological image processing method) is used to remove the noise and get the binarization image, as shown in Fig. 8.

C. Extraction of Dynamic Target Center by Median Method

It is difficult to track dynamic targets for many reasons. For example, there is relative motion velocity between the satellite and dynamic target, meanwhile, imaging has certain ambiguity, the whole feature matching is complex calculated, and all of them lead to a lot of errors. Therefore, the median method which is also called area equality method is used to extract the center of dynamic target as the target-missing quantity to guide satellite tracking. With this method, the area of the image in X direction and Y direction is equal. The formulas are expressed as follows:

Fig. 8. Binary Processing Chart of Aircraft. (a) Original area of the aircraft; (b) Binary image of the aircraft.

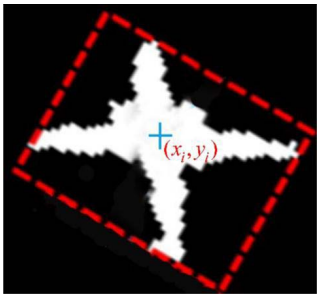

Fig. 9. Target-missing quantity extracted from the center of aircraft.

$$Q(x) = \sum_{x_{\min}}^{x} \sum I(x, y) \tag{14}$$

$$Q(x_i) = \frac{1}{2}[Q(x)_{\max} - Q(x)_{\min}] \tag{15}$$

$$Q(y) = \sum_{y_{\min}}^{y} \sum I(x, y) \tag{16}$$

$$Q(y_i) = \frac{1}{2}[Q(y)_{\max} - Q(y)_{\min}] \tag{17}$$

where Q is the area occupied by aircraft, (x_i, y_i) represents the center coordinate of the object in two-dimensional image, as shown in Fig. 9. When a dynamic target is captured, different black-and-white aircraft images are obtained by binary image processing, and then target-missing quantity (+) is extracted from the center of the dynamic target by using the median method.

D. Attitude Deviation Between Target Center and Optical Axis

The two-dimensional attitude deviations between target-missing quantity and optical center are determined by the

focal length of camera f, the pixel size of Complementary Metal Oxide Semiconductor (CMOS)A and the target position located in image. The corresponding formulas of the attitude deviation are shown as follows.

$$\begin{cases} \Delta\theta = (x_1 - x_0) \times A/f \\ \Delta\varphi = (y_1 - y_0) \times A/f \end{cases} \tag{18}$$

IV. Terminal Sliding Method for Tracking

When optical satellite is tracking dynamic target, the terminal sliding control algorithm is adopted to achieve stable imaging. It uses the nonlinear function of sliding hyperplane to replace the linear sliding mode surface in the traditional structure. Therefore, the tracking error of system which is located on the sliding mode surface can be converted to zero within a finite time, thus making the process of imaging more accurate. The dynamics and kinematics equations of satellite are expressed as follows: [20]:

$$\begin{aligned} \dot{\rho} &= \frac{1}{4}\left[\left(1 - \rho^T\rho\right) I_{3\times3} + 2\tilde{\rho} + 2\rho\rho^T\right]\omega \\ &= F(\rho)\,\omega = f_1(\rho, \omega) \end{aligned} \tag{19}$$

$$\begin{aligned} \dot{\omega} &= -J^{-1}\omega \times (J\omega) + J^{-1}u + J^{-1}T_{ext} \\ &= f_2(\rho, \omega) + Bu + J^{-1}T_{ext} \end{aligned} \tag{20}$$

where ρ represents the modified Rodrigues parameter (MRP), $\tilde{\rho}$ is the skew-symmetric matrix of ρ, ω is the attitude angular velocity of satellite, J represents the moment of inertia of satellite, B is the inverse matrix of J, u is the control moment, and T_{ext} is the external interference moment.

According to the terminal sliding control method and Lyapunov stability theory, the form of control moment can be expressed as follows [21]:

$$\begin{aligned} u = &-b^{-1}\left[f - \ddot{\rho}_d - \ddot{p} + C_2^{-1}C_1\left(\dot{\rho}_e - \dot{p}\right)\right] \\ &-b^{-1}\left(K\frac{C_2^T\sigma}{\left\|C_2^T\sigma\right\| + \delta_0 + \delta_1\left\|\rho_e\right\|} + \frac{\partial f_1(\rho,\omega)}{\partial\omega}J^{-1}D\right) \end{aligned} \tag{21}$$

$$f = \frac{\partial f_1(\rho,\omega)}{\partial\rho}f_1(\rho,\omega) + \frac{\partial f_1(\rho,\omega)}{\partial\omega}f_2(\rho,\omega) \tag{22}$$

$$b = \frac{\partial f_1(\rho,\omega)}{\partial\omega}B \tag{23}$$

where, $\sigma = CE - W(t)$ denotes the surface function of the sliding control, it is also a combination of the control deviation and the relative parameters of satellite. ρ_d represents the target attitude, ρ_e is the error MRP parameter, D is the upper limit of T_{ext}, t represents time, $C_i = diag(c_{i1}\ c_{i2}\ c_{i3})$ is the positive constant, and K, δ_0, δ_1 represent constants, respectively.

According to the above models, the form of the sliding surface function can be expressed as follows:

$$\begin{aligned} E &= \begin{pmatrix} \rho_e \\ \dot{\rho}_e \end{pmatrix} = (\rho_{1e}, \rho_{2e}, \rho_{3e}, \dot{\rho}_{1e}, \dot{\rho}_{2e}, \dot{\rho}_{3e})^T \\ W(t) &= CP(t) \\ P(t) &= \begin{pmatrix} p \\ \dot{p} \end{pmatrix} \\ C &= \begin{pmatrix} C_1 & C_2 \end{pmatrix} \end{aligned}$$

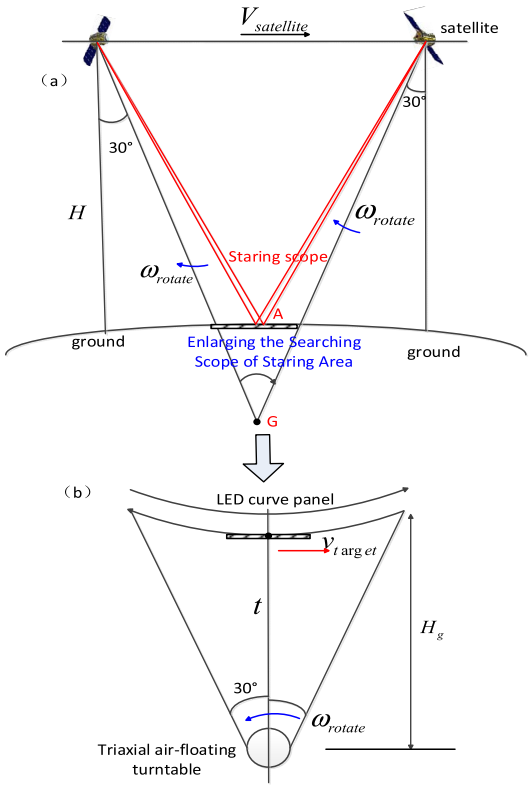

Fig. 10. Enlarging the searching scope of staring area (a) On-orbit; (b) Ground experiment.

$$\begin{aligned} p(t) = &\rho_e(0) + \dot{\rho}_e(0)\,t + \frac{1}{2}\ddot{\rho}_e(0)\,t^2 \\ &+\left[\frac{-10}{T^3}\rho_e(0) + \frac{-6}{T^2}\dot{\rho}_e(0) + \frac{-3}{2T}\ddot{\rho}_e(0)\right]t^3 \\ &+\left[\frac{15}{T^4}\rho_e(0) + \frac{8}{T^3}\dot{\rho}_e(0) + \frac{3}{2T^2}\ddot{\rho}_e(0)\right]t^4 \\ &+\left[\frac{-6}{T^5}\rho_e(0) + \frac{-3}{T^4}\dot{\rho}_e(0) + \frac{-1}{2T^3}\right]t^5 \end{aligned} \tag{24}$$

This method inherits the general characteristics of the sliding control strategy. The whole control system can achieve the expected attitude in a short time, and maintain good stability and robustness. The control law of satellite can guarantee the global asymptotic stability of the control system, and control satellite tracking and pointing to dynamic targets.

V. Ground Experiment and On-Orbit Demonstration

Due to the high investment and risk of satellite imaging systems, it is necessary to carry out strict experiments on the ground to verify the correctness of the technology. In ground simulation system, the CMOS system is equivalent to camera, the control system of triaxle platform is equivalent to satellite, the large LED (light emitting diode) panel is equivalent to the surface of earth. The COMS system is fixed on the triaxle platform to search and track dynamic target of the LED panel as the satellite moves.

A. Ground Experiment

The process of satellite imaging is shown in Fig. 10, and the ground experiment equipment is shown in Fig. 11.

Fig. 11. Ground experiment equipment of enlarging the searching scope of staring area and tracking imaging of dynamic targets.

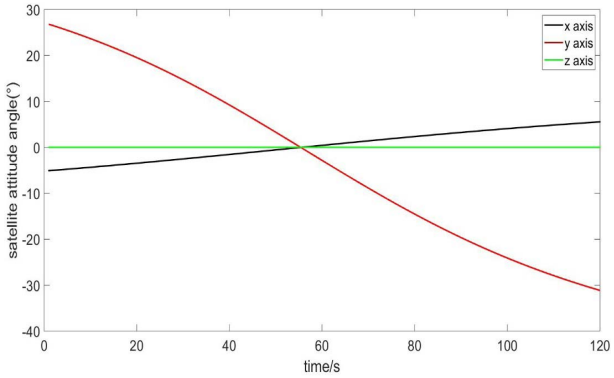

Fig. 12. Triaxle Euler angle in tracking experiment.

$V_{satellite}$ is the flight velocity of satellite, ω_{rotate} is rotational Euler angular velocity of satellite, v_{target} is velocity of the target, and H is the altitude of the satellite. According to the size of LED panel, when the object distance H_g is 5 m, the three-axis air-floating turntable can maneuver with a pitch angle ± 30 ° and a roll angle ± 25 °. In ground experiment, the control platform of satellite consists of triaxle air-floating turntable, flywheel, optical fiber gyroscope, CPU, dynamic target, tilt sensor. The parameters of the ground experiment are shown in Table I. The focal length of the camera is 7 mm, the pixel size of CMOS is 7μ m, and the exposure time is in the range of 0.1ms ∼20ms. The size of the curved LED panel is 6 m ×4 m, the radius of the panel is 32 m and the pixel size of LED is 5 mm (Abbreviated as P5). Then the coordinate system of the three-axis air-floating turntable, in which x-axis points to the LED large panel, and z-axis is perpendicular to the turntable can be defined.

Due to the limited distance on the ground and the pixel size of CMOS, it is impossible to obtain the same angular resolution and relative velocity. The ability of the satellite attitude control system, the expansion effect of the satellite gaze search range, the target miss distance extraction from object and the influence on the platform can be verified in the ground experiment.

B. Attitude Control Experiment

Firstly, the dynamic target is displayed in LED large panel. According to the algorithm, the three-axis air flotation turntable carries out attitude maneuver control, and the camera

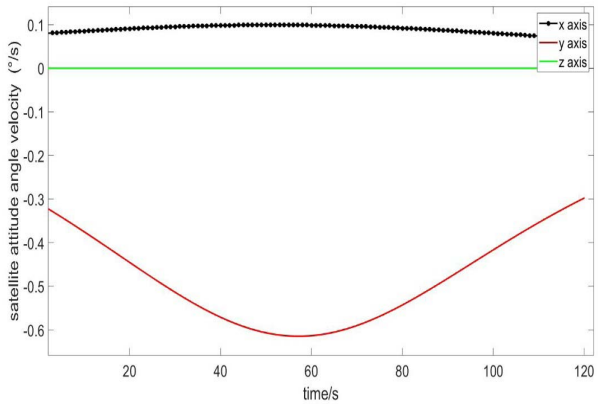

Fig. 13. Triaxle Euler angular velocity in tracking experiment.

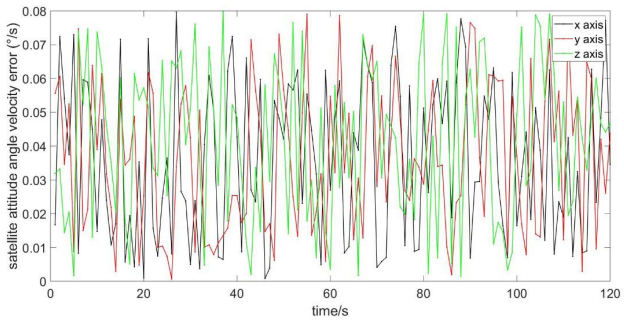

Fig. 14. Tracking error results of Triaxle attitude angle velocity in experiment.

Fig. 15. The image of conventional staring imaging in experiment (pixel size 600 × 600).

carries out real-time search imaging for LED. If dynamic target is found, the platform will track it in real time according to target-missing quantity. The moment of triaxle air-floating turntable is

$$I = \begin{bmatrix} 7.5 & -0.2 & 0.1 \\ -0.2 & 10.3 & -0.15 \\ 0.1 & -0.15 & 11 \end{bmatrix} \tag{25}$$

When the control period is 1 Hz, the triaxle Euler angle obtained through the experiment is shown in Fig. 12, and the triaxle Euler angular velocity is shown in Fig. 13. According to the experiment, when the satellite is tracking, the air floating platform can achieve attitude stability better than 0.08 °/s and pointing accuracy better than 0.05 °, the corresponding results are shown in Fig. 14.

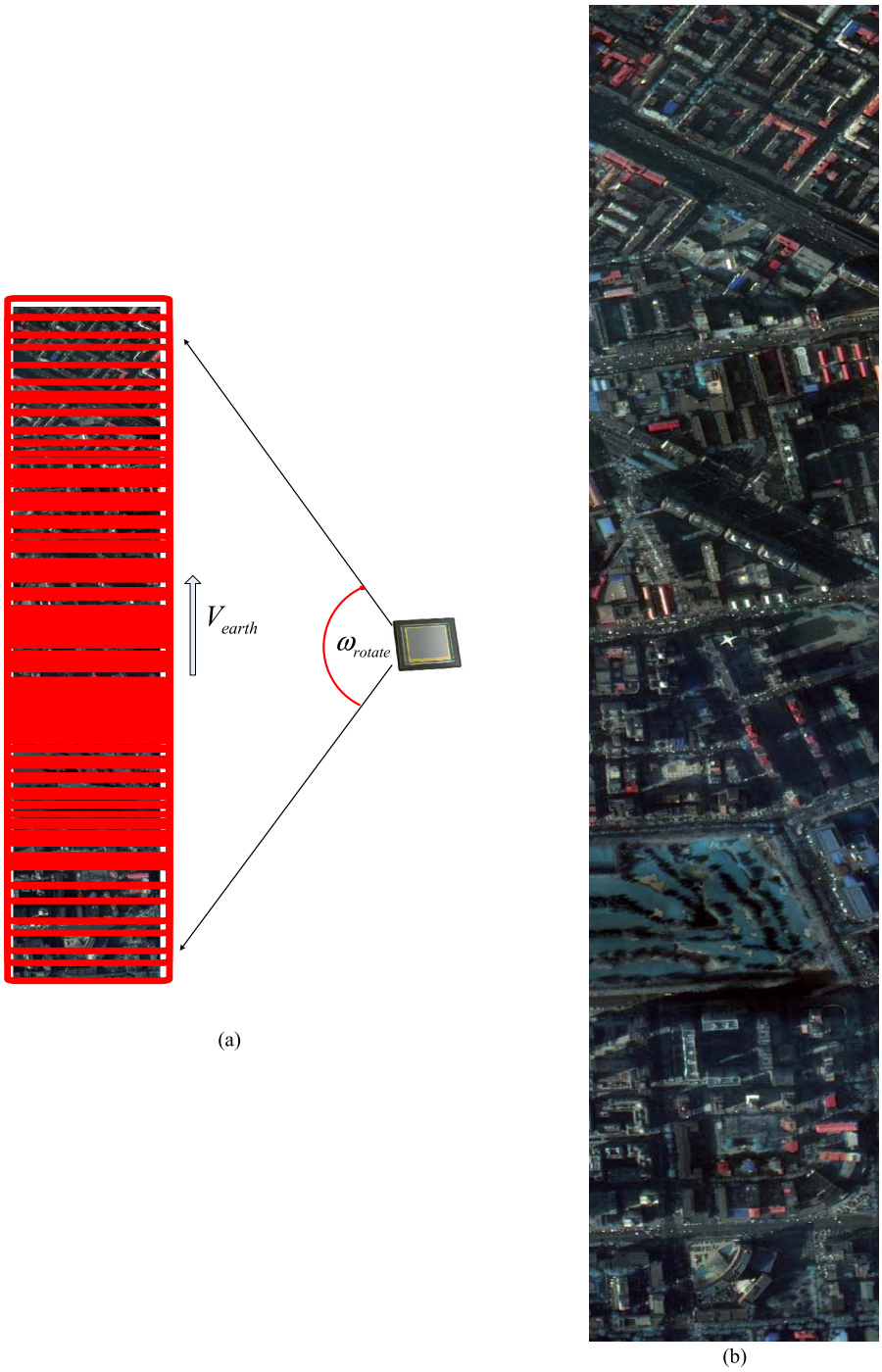

Fig. 16. The image of the expanded search imaging in experiment (pixel size 4735 × 600). (a) The experiment image with consecutive frames; (b) The experiment image.

When the orbit height of the satellite is 500 km, the deviation range corresponding to the pointing accuracy of 0.05° is 0.434km (500000 m $\times 0.05° \times \pi/180$). For the imaging range of tens of kilometers or hundreds of kilometers, the dynamic target can still be searched, so the pointing accuracy meets the requirements; When the attitude stability of the satellite is 0.08°/s and the exposure time of the camera is 0.1ms, the image movement corresponding to the exposure time is 0.07m(500000m $\times 0.08° \times \pi/180 \times 0.0001$ s), which is equivalent to a deviation of 0.14 pixels, and then the image will not be blurred. In this case, the actual amplitude of the control torque of the satellite is very small, which can meet the requirements of on-orbit verification task.

C. Imaging Experiment Analysis

1) The Expansion Effect of the Satellite Gaze Search Range: In the process of ground simulation imaging, when the camera is in conventional staring imaging, the imaging range corresponding to the field of view is 600 pixels × 600 pixels, as shown in Fig. 15.

As the virtual target point is set, the turntable takes maneuver imaging according to the attitude angle curve of Fig.12

TABLE I
GROUND EXPERIMENT PARAMETERS

Serial number	Ground experiment parameters	Value
1	Curvature radius of LED panel	32 m
2	Focal length of camera	7 mm
3	Pixel size of CMOS	7 μm
4	Object distance	5 m
5	Pixel size of LED (Imaging resolution)	5 mm
6	Pitch angle	±30 °
7	Pitching angular velocity of turntable	-0.3 °/s~-0.65 °/s
8	Roll angular velocity of turntable	0.08 °/s ~0.15 °/s
9	Yaw angular velocity of turntable	-0.03 °/s ~0.05 °/s
10	Target movement speed	0.35 m/s
11	Size of LED panel	6 m×4 m
12	Length of imaging time	75 s

Fig. 17. Tracking dynamic target in experiment.

Fig. 18. Tracking dynamic extraction.

and the attitude angle velocity of Fig.13 during simulation imaging. The total time is about 75s. Calculated from the range in the direction of staring search, the corresponding length of imaging is about 4735 pixels([(0.35m/s ×75s-0.6°/s ×75s ×5m/57.3)/0.005]) in its pitch direction. The searching area can be expanded to 4735 pixels ×600 pixels. Compared with other methods, it is no longer necessary to divide the imaging strip area and build the overlap rate of consecutive frame, but the imaging range can be expanded 8 times, as shown in Fig. 16.

2) The Target Miss Distance Extraction From Object and the Influence on the Platform: The SIFT method is applied to quickly match the aircraft image, which can quickly identify the aircraft target in the image, as shown in Fig. 17. Then, the method of binarization processing and extraction of dynamic target center by median are used to quickly process the target, as shown in Fig. 18 and Fig. 19. And then the location distance between the miss distance and the center of the field of view are determined, as shown in Fig. 20. The corresponding positions of the center of the FOV and the center of the miss distance are calculated with ($x_0 = 300$, $y_0 = 300$) and ($x = 284$, $y = 353$), respectively.

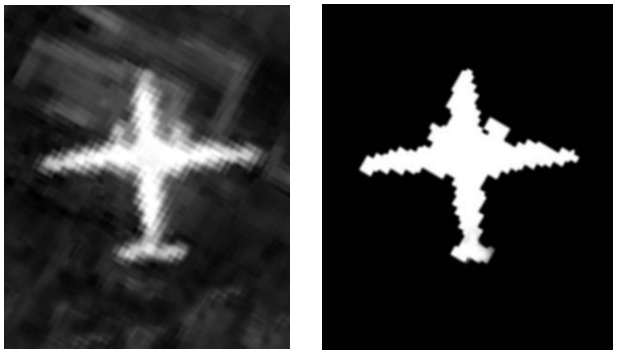

(a) (b)

Fig. 19. Binary Processing Chart of aircraft. (a) Original area of the aircraft; (b) Binary image of the aircraft.

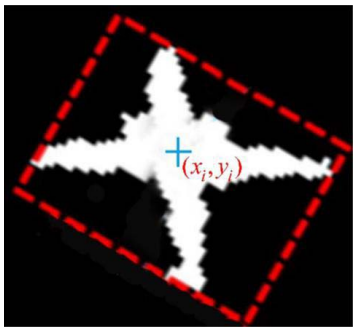

Fig. 20. Target-missing quantity extracted from the center of aircraft.

At this time, the pixel size and camera focal length of the satellite are substituted to obtain the introduced attitude error that the satellite needs to track. The attitude deviation of the satellite is calculated as follows:

$$\begin{cases} \Delta\theta = (x_1 - x_0) \times A/f = -16 \times 0.000007/7 \approx 0.001^\circ \\ \Delta\varphi = (y_1 - y_0) \times A/f = -53 \times 0.000007/7 \approx 0.003^\circ \end{cases} \tag{26}$$

According to the calculated deviation attitude, it can be seen that only a small deviation adjustment is needed in the staring search imaging process. It means that the dynamic target can be followed up and the satellite attitude control system will not be affected.

Based on the inherent characteristics of the moving target, the dynamic target recognition is completed and the target-missing quantity is calculated in the experiment. According to the target-missing quantity, the real-time tracking of the satellite maneuver is completed. Finally, the dynamic aircraft searching and tracking can be well completed on the ground experiment.

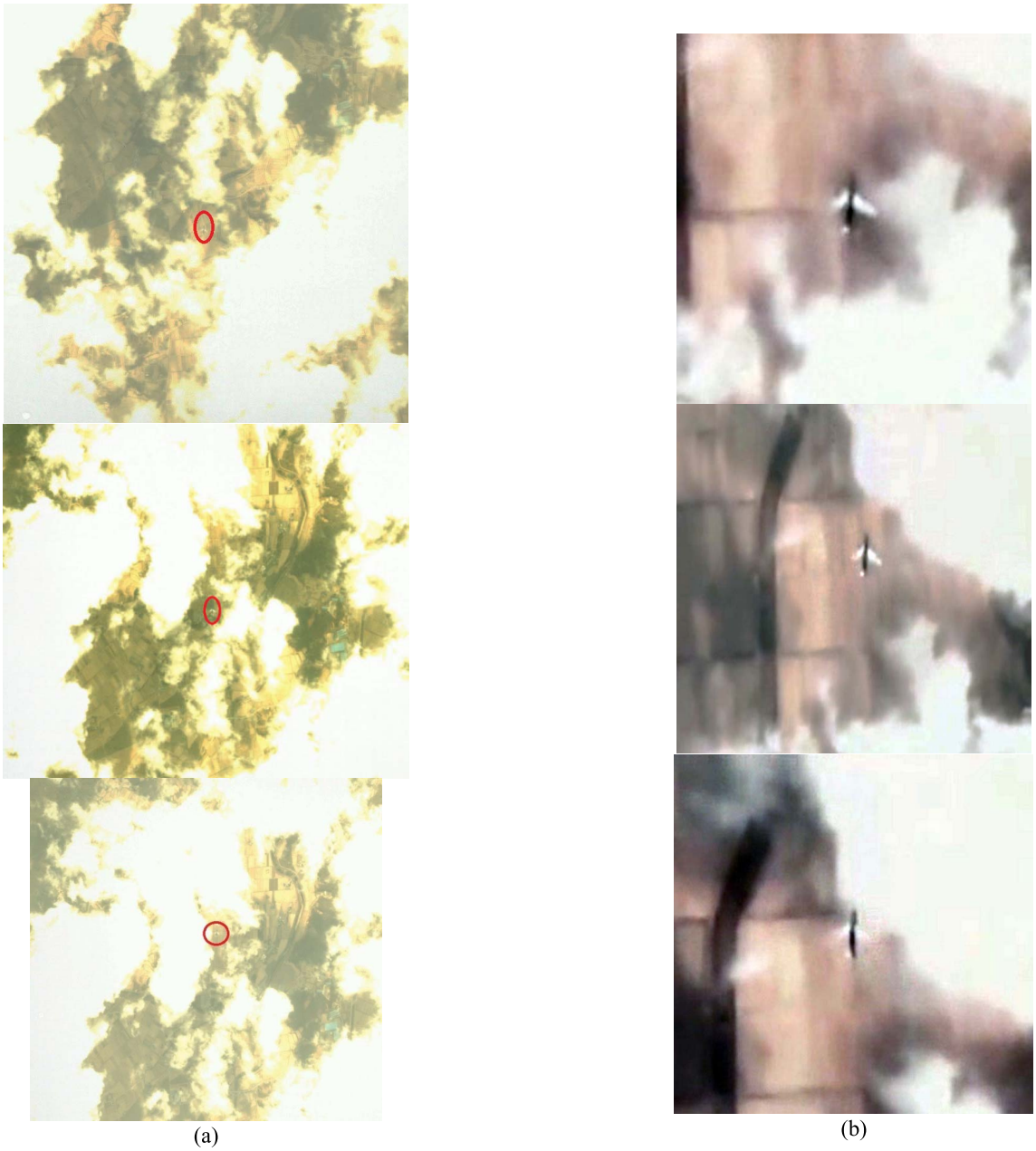

(a) (b)

Fig. 21. Expanded searching and tracking of on-orbit dynamic aircraft. (a) Satellite expanded searching on-orbit; (b) Satellite real-time tracking imaging of dynamic aircraft.

D. The Extended Search and Tracking Imaging of Dynamic Aircraft on-Orbit

In order to verify the theory of this paper, JL-1(The first commercial remote sensing satellite in Jilin Province) optical video satellite applies this method to search and track dynamic target in the airport area. JL-1 satellites were launched at 12:13 on October 7, 2015 in Jiuquan. The video satellite of JL-1 four-satellite group was carried by the changzheng-2d launch vehicle into the sun synchronous orbit. The orbit altitude is 656km and the local time of descending point is 10:30. The envelope size of satellite payload is 1120 mm × 463 mm × 1050 mm; and flywheels are used in the attitude control system as the major executive mechanism to execute staring tracking control, whose maximum angular velocity for attitude maneuver is 2 °/s, and the stability of maneuver process is 0.005 °/s. The mass of video satellite is less than 95 kg. The payload of video satellite is 5.5μm in pixel size, 3.2 m in focal length and 4.6 km in ground coverage, as shown in Table II.

JL-1 optical video satellite adopted this method to carry out the on-orbit test of expanded searching and real-time tracking of dynamic targets in the area of Dandong airport in October 21. JL-1 video satellite has achieved the expansion of search range in key areas as shown in Fig. 21(a), the imaging object is an aircraft over the cloud, and the exposure time is 0.2ms [22]. The scope of imaging which is nearly seven times larger than the scope of conventional gaze imaging. In addition, it has identified a real-time flying aircraft in the area. After the target-missing quantity is extracted, the satellite completes the real-time acquisition and follow-up tracking

TABLE II
IMAGING PARAMETERS ON-ORBIT

Serial number	Imaging parameters on-orbit	Value
1	maximum attitude maneuver angular velocity	2 °/s
2	stability of maneuver	0.005 °/s
3	pixel size	5.5 μm
4	focal length	3.2 m
5	Field of view	1.2°
6	Image size	4096×3072
7	Mass of payload	22kg
8	Power Consumption	18W

of the on-orbit dynamic aircraft, as shown in Fig. 21(b). According to the variation and time difference of the inter frame images, the flight velocity of the aircraft is estimated to be 840km/h. Due to the errors of imaging time accuracy and pixel registration, there is a certain amount of deviation in velocity calculation. However, the target aircraft in orbit imaged is a non-cooperative target, so it is impossible to verify the estimated velocity accuracy.

VI. CONCLUSION

In summary, we have proposed an expanded searching and tracking method for dynamic targets. The attitude-guided equation based on target-missing quantity can achieve fast capturing and tracking of dynamic targets. The method can provide technical support for researching the flight characteristics of dynamic targets. In the future, we will study the applicability of the algorithm in different geomorphologic areas based on more samples of the imaging area, and try to use image enhancement technology to improve the accuracy of imaging recognition and real-time tracking.

REFERENCES

[1] S. Franks, J. G. Masek, and M. G. Turner, "Monitoring forest regrowth following large scale fire using satellite data—A case study of yellowstone national park, USA," *Eur. J. Remote Sens.*, vol. 46, no. 1, pp. 551–569, Jan. 2013.

[2] P. Boccardo and F. G. Tonolo, "Remote sensing role in emergency mapping for disaster response," *Engineering Geology for Society and Territory*, vol. 5. Berlin, Germany: Springer, 2015, pp. 17–24.

[3] X. N. Niu, H. Tang, and L. X. Wu, "Multi-satellite observation scheduling for large area disaster emergency response," *ISPRS Int. Arch. Photogramm., Remote Sens. Spatial Inf. Sci.*, vol. XLII-3, pp. 1327–1331, Apr. 2018.

[4] S. Sowmya and R. Somashekar, "Application of remote sensing and geographical information system in mapping forest fire risk zone at Bhadra wildlife sanctuary, India," *J. Environ. Biol.*, vol. 31, no. 6, p. 969, 2010.

[5] C. Mielke, N. Boesche, C. Rogass, H. Kaufmann, C. Gauert, and M. de Wit, "Spaceborne mine waste mineralogy monitoring in south africa, applications for modern push-broom missions: Hyperion/OLI and EnMAP/Sentinel-2," *Remote Sens.*, vol. 6, no. 8, pp. 6790–6816, Jul. 2014.

[6] M. Wang, C. Chen, J. Pan, Y. Zhu, and X. Chang, "A relative radiometric calibration method based on the histogram of side-slither data for high-resolution optical satellite imagery," *Remote Sens.*, vol. 10, no. 3, p. 381, Mar. 2018.

[7] G. Easson, S. DeLozier, and H. G. Momm, "Estimating speed and direction of small dynamic targets through optical satellite imaging," *Remote Sens.*, vol. 2, no. 5, pp. 1331–1347, May 2010.

[8] J. R. Irons, J. L. Dwyer, and J. A. Barsi, "The next landsat satellite: The landsat data continuity mission," *Remote Sens. Environ.*, vol. 122, pp. 11–21, Jul. 2012.

[9] L. Yin, X. Wang, and Y. Ni, "Flexible three-dimensional reconstruction via Structured-Light-based visual positioning and global optimization," *Sensors*, vol. 19, no. 7, p. 1583, Apr. 2019.

[10] M. Etaya, T. Sakata, H. Shimoda, and Y. Matsumae, "An experiment on detecting moving objects using a single scene of QuickBird data," *J. Remote Sens. Soc. Jpn.*, vol. 24, no. 4, pp. 357–366, 2003.

[11] W. Ya-min *et al.*, "Design of pendulum type searching imaging along the track long-strip with high resolution CMOS camera," *Acta Photonica Sinica*, vol. 46, no. 3, 2017, Art. no. 311002.

[12] P. Tangpattanakul, N. Jozefowiez, and P. Lopez, "A multi-objective local search heuristic for scheduling Earth observations taken by an agile satellite," *Eur. J. Oper. Res.*, vol. 245, no. 2, pp. 542–554, Sep. 2015.

[13] J. R. Wertz, *Spacecraft Attitude Determination and Control*. Berlin, Germany: Springer, 2012.

[14] Z. Renwei, *Dynamics and Control of Satellite Orbit and Attitude*. Beijing, China: Beijing Univ. Aeronautics and Astronautics Press, 1998.

[15] J. Bingqiang, Y. Dong, and S. Zhaowei, "Trajectory optimization for satellite fast attitude maneuver based on collocation method," in *Proc. Int. Conf. Mechatronics Control (ICMC)*, Jul. 2014, pp. 1294–1298.

[16] T. Kouyama, A. Kanemura, S. Kato, N. Imamoglu, T. Fukuhara, and R. Nakamura, "Satellite attitude determination and map projection based on robust image matching," *Remote Sens.*, vol. 9, no. 1, p. 90, Jan. 2017.

[17] J. Wang, P. Yu, C. Yan, J. Ren, and B. He, "Space optical remote sensor image motion velocity vector computational modeling," *Acta Optica Sinica*, vol. 24, no. 12, pp. 1585–1589, 2004.

[18] D. G. Lowe, "Distinctive image features from scale-invariant keypoints," *Int. J. Comput. Vis.*, vol. 60, no. 2, pp. 91–110, Nov. 2004.

[19] T. Lindeberg, "Scale invariant feature transform," *Scholarpedia*, vol. 7, no. 5, 2012, Art. no. 10491.

[20] S.-C. Lo and Y.-P. Chen, "Smooth sliding-mode control for spacecraft attitude tracking maneuvers," *J. Guid., Control, Dyn.*, vol. 18, no. 6, pp. 1345–1349, Nov. 1995.

[21] M. S. Branicky, "Multiple Lyapunov functions and other analysis tools for switched and hybrid systems," *IEEE Trans. Autom. Control*, vol. 43, no. 4, pp. 475–482, Apr. 1998.

[22] W. Xu, G. Jin, and J. Wang, "Optical imaging technology of JL-1 lightweight high resolution multispectral remote sensing satellite," *Opt. Precis. Eng.*, vol. 25, no. 8, pp. 1969–1978, 2017.

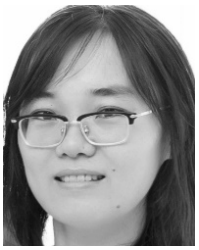

Li Jiang was born in Songyuan, Jilin, in 1984. She received the B.S. and M.S. degrees in physics and the Ph.D. degree in optical engineering from Jilin University, Changchun, China, in 2008 and 2011, respectively.

From 2011 to 2017, she was an Assistant Professor with the College of Science, Changchun University of Science and Technology, China. Since 2018, she has been an Associate Professor with the Physics Department. She is the author of 15 articles and 12 inventions. Her research interests include dynamic target tracked imaging by Space-based payload and the imaging simulation of space optical remote sensing.

Xiubin Yang was born in Fusong, Jilin, in 1982. He received the B.S. degree in physics from the University of Nankai, Tianjin, in 2006, and the Ph.D. degree in optical engineering from the Chinese Academy of Science University, Changchun, in 2011.

From 2013 to 2019, he was an Associate Professor with The Space-based Dynamic and Rapid Optical Imaging Laboratory. Since 2020, he has been a Professor with The Space New Technique Department, Changchun Institute of Optics, Fine Mechanics and Physics, Chinese Academy of Sciences. He is the author of two books, 32 articles, and 36 inventions. His research interests include dynamic imaging process of space optical camera, new mode of optical imaging, and advanced optical payload technology.

Mr. Yang was a recipient of the second prize of China National Science and Technology Progress Award in 2017, the first prize of provincial science and technology progress award in 2014, and the Seventh Outstanding Contribution Award of Changchun city in 2018.